# Effects of Cap Gap and Spiral-Welded Seam Composite Defects on Concrete-Filled Steel Tubes


**Zhengran Lu, Chao Guo, and Guochang Li**

**Abstract** Many old concrete-filled steel tube (CFST) arch bridges use consisted of ordinary concrete and spiral-welded steel tubes. However, low strength of spiral-welded seams (SWS) and cap gaps of concrete due to fluidity composed composite defects in CFST arch bridges. In the current work, a finite element analysis has been performed using ultrasonic scanning field tests on the bearing capacity of a serviced CFST arch bridge rib with a cap gap and reduced SWS strength exposed to a weak eccentric axial compression. The nonlinear behaviors of different components and composite defect influence on CFST performance were also studied. Composite defect influences on the bearing capacity of CFSTs were also experimentally studied. This research proposed a theoretical analysis method for the maintenance and restoration strategy of CFST arch bridges.

**Keywords** Concrete-filled steel tube · Bearing capacity · Gap · Composite defect · Nonlinear finite element analysis

## 1 Introduction

In previous decades, many imperfections have been formed in concrete core columns (CCC) and steel tubes of several concrete-filled steel tube (CFST) arch bridges in China during their initial manufacturing or service life [1]. During the last two decades, a large number of experimental and numerical research works have been performed on CFST columns exposed to axial loadings through finite element analysis (FEA). Han et al. [2] and Ellobody and Young [3] carried out elastic-to-plastic FEA on CFST columns having circular or square sections. Hassanein [4], Tao et al. [5, 6], and Ellobody and Young [7] conducted nonlinear FEA on short or long CFST columns. Hu and Su [8] and Huang et al. [9] applied ABAQUS software to analyze CFST column strength performance. Most of the above analyses focused on small-diameter CFSTs, whether straight-welded or seamless, without considering

Z. Lu · C. Guo (✉) · G. Li
School of Civil Engineering, Shenyang Jianzhu University, Shenyang, China
e-mail: guochaoglovel@126.com



Y. Li et al. (eds.), *Advances in Simulation and Process Modelling*,
Advances in Intelligent Systems and Computing 1305,
https://doi.org/10.1007/978-981-33-4575-1_29

the effects of concrete gap, SWS strength and segregation defects on the bearing performance of these structures. On the other hand, in existing CFSTs, especially large-diameter CFST arch bridges constructed twenty years ago, have inevitably been influenced by the mentioned defects. Liao et al. [10, 11], Han et al. [12], Huang et al. [13] have previously studied single-factor CFST rib defects. However, there few studies have been conducted on cap gap and SWS composite defects on CFSTs. In the current research, a CFST arch bridge was considered as research object and cap gaps and SWS were assumed as composite defects acting on CFST arch bridge ribs. To do so, a series of nonlinear FEA analyses were performed on CFST rib members with cap gaps and SWS composite defects under eccentric axial compression.

## 2 Problem Statement

This paper aimed to study the CFST arch bridge of Chang-Qing Hun River Bridge located in Shenyang City, Liaoning Province in northern China (Fig. 1).

The bridge was built in 1997 and has 120 + 140 + 120 m net span. Arch cross-sectional height and width are 2.4 and 1.8 m, respectively. Each of the ribs is consisted of 4 tubes 720 mm in diameter; spiral-welded tube (SWT) thickness is 10 mm. All K-shape, transverse, and lateral braces have similar diameter to the main rib. SWT was constructed by welding the aligned edges of curved spiral steel plates. However, the welded seam strength of SWTs was lower than that of base metal; spiral-welded seam (SWS) penetrated only about 70% [14, 15]. Today, self-consolidating concrete (SCC) is used in CFSTs because of its convenience of construction. Despite its importance, before 2001, i.e., 4 years after the construction of the above bridge was completed, no research work had been conducted on SCC application in CFST arch bridges in China [16]. As a result, ordinary concrete was employed in this bridge. Therefore, in concrete pouring process, cap gaps could be easily created at concrete-steel tube interface, particularly on the top arch rib. For the determination of real existing defects on CFST arch ribs, a 3D ultrasonic section scanning imager (MIRA A1040, ACSYS, Russia) was used to detect defects.

The results showed that the ratio of interface gap to total tube areas was in the range of 3.6–30.5% and the depth of cap gap was about 15–45 mm. Based on the

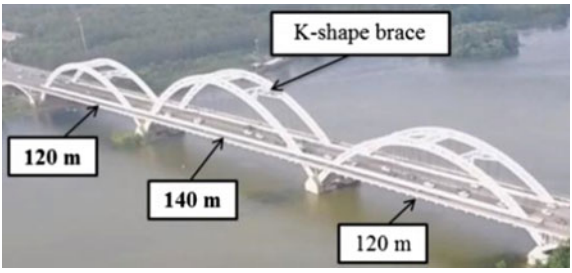


**Fig. 1** Chang-Qing Hun River Bridge

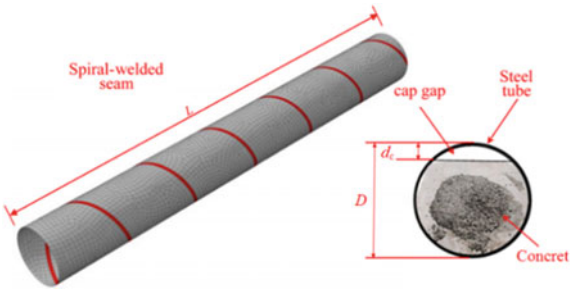


**Fig. 2** Mesh of CFST composite defects

ultrasonic data, FEAs were developed for analytical investigation and estimation of cap gaps and SWS, in which section gap ratio ($\chi$) was the most important calculation parameter:

$$\chi = \frac{d_c}{D} \tag{1}$$

where, as shown in Fig. 2, $D$ is SWT section outer diameter and $d_c$ is the size of cap gap and is specified as the maximum distance between CCC and SWT inner surface.

## 3 Methods

FEAs were performed by ABAQUS software, and SWT was simulated by a 4-node simplified integrating shell element (S4R). Also, CCC was considered as an 8-node hexahedral element (C3D8) with each node having 3 translational degrees of freedom [17, 18]. The loading eccentricity was $D/6$ and steel tube $\sigma - \varepsilon$ relationship in CFST members conformed to the trilinear material property model proposed by Tao and Wang [19]. In this case, steel tube parameters are given in Table 1.

The concrete core was drilled from serviced CFST of Chang-Qing Hun River Bridge to obtain the real strength grade of CCC using unconfined compressive strength tests. Based on the obtained results, Poisson's ratio $\mu_c$, cylinder compressive strength $f'_c$, and corresponding strain $\varepsilon'_c$ values of concrete specimens 100 mm in diameter exposed to uniaxial compressive stress were found to be 0.21, 33 MPa, and 0.0033, respectively. $E_c$ was calculated using the experimental Eq. (2) suggested in ACI318 [20] to be $2.7 \times 10^4$ MPa, in which $f'_c$ is in MPa.

**Table 1** Steel tube parameters

| $t$ mm | $D$ mm | $E_s$ MPa | $\mu_s$ | $f_y$ MPa | $f_u$ MPa | $\varepsilon_y$ | $\varepsilon_u$ |
|---|---|---|---|---|---|---|---|
| 10 | 700 | $2.0 \times 10^5$ | 0.32 | 345 | 400 | 0.00192 | 0.179 |

$\mu_s$ Poisson's ratio, $D$ outer diameter, $t$ thickness

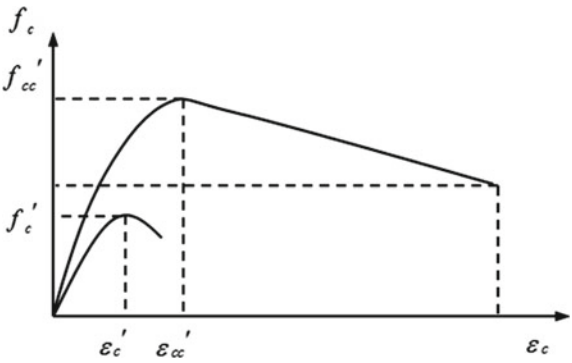


**Fig. 3** Stress–strain curve

$$E_c = 4700\sqrt{f_c'} \tag{2}$$

According to the experimental results reported in [21], the following equation was developed for the prediction $f_{bc}/f_c'$ ratio as 1.12:

$$f_{bc}/f_c' = 1.5\left(f_c'\right)^{-0.075} \tag{3}$$

where $f_{bc}$ denotes initial equibiaxial compressive yield stress. In case, core concrete was exposed to circular confining pressures, uniaxial compressive yield strength $f_c'$ and corresponding strain $\varepsilon_c'$ (Fig. 3) were considerably greater than those obtained for unconfined concrete. Mander et al. [22, 23] estimated -$\varepsilon_{cc}' - \varepsilon_c'$ and $f_{cc}' - f_c'$ relations. Han et al. [24] applied Mander's model to develop equivalent $\sigma - \varepsilon$ model for the simulation of CCC plastic behavior in CFSTs, as shown in Fig. 3.

## 4 Results and Discussion

### *4.1 FEA of CFST with SWS Defect*

In FEA, the strength values of SWS were 50, 70, and 100% of those of parent materials. The length $L$ and screw pitch of seam were 3 and 0.95 m, respectively. For the evaluation of SWS strength effect on the bearing capacity of CFSTs, firstly, empty steel tube (EST) was investigated and then, CFST was evaluated, as shown in Fig. 4, which presents the comparison of $N - \varepsilon$ curves drawn for ESTs in the presence and absence of SWS defects. It was seen in Fig. 4a that, after reaching yield strength, $N$ in ESTs with or without SWS defects appeared strain-softening until reaching a high axial strain ($\varepsilon = 0.03$).

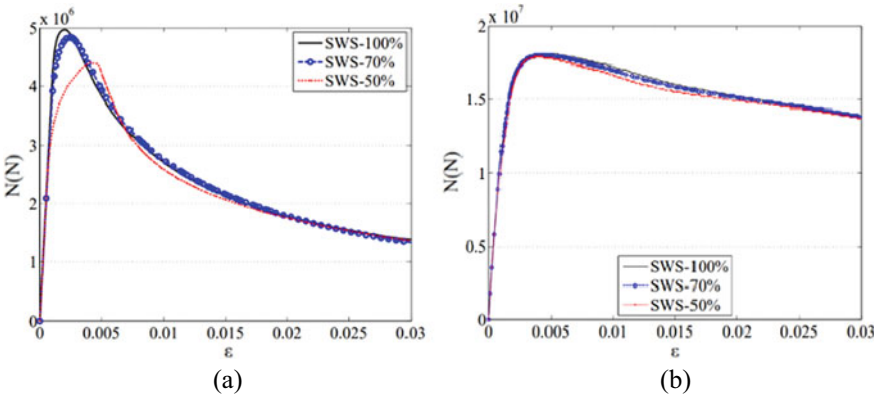


**Fig. 4** Comparison of $N - \varepsilon$ relationships. **a** EST, **b** CFST

However, 30 and 50% strength loss due to SWS defects decreased the strength of EST by 2.6% and 11.2%, respectively, which led to strain-softening ability reduction. It was concluded that EST strength loss due to SWS defects was mainly because of decrease in strength contribution.

As seen in Fig. 4b, under different SWS defect conditions, CFST $N - \varepsilon$ curves were almost similar. The results showed that when inner concrete had no defects, the decrease of EST strength with SWS defects had only a slight effect on the bearing capacity of CFST. This was consistent with experiences in references [14] and [15]. Figure 5 compares typical EST deformation modes. When SWS strength was less than that of base metal, SWS exhibited local buckling on EST compression side. By decreasing the intensity of SWS, this phenomenon became more obvious.

Figure 6 compares typical CFST SWT failure modes. The results showed that CFST outer SWT strength was reduced at weld seam, but it was different from the local fold buckling failure modes of EST.

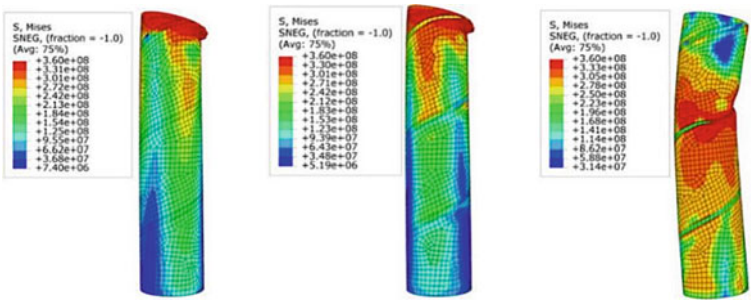


**Fig. 5** EST von Mises stresses (Pa) with different SWS strengths. **a** SWS: 100%, **b** SWS: 70%, **c** SWS: 50%

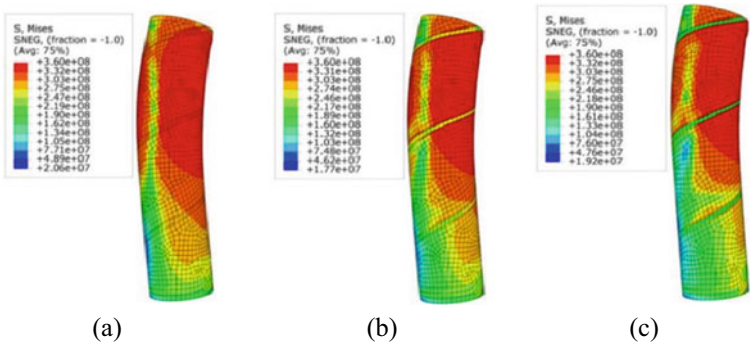


**Fig. 6** Tube Mises stresses (Pa) in CFSTs with various SWS strengths. **a** Tube SWS: 100%, **b** Tube SWS: 70%, **c** Tube SWS: 50%

In addition, it was proved that CCC had strong restraint ability. If CCC had no defects, it could fully support outer steel pipe and prevent local buckling. Therefore, coinciding performance of concrete and steel tube was ensured.

## *4.2 FEA of CFST with Cap Gap Defect*

Figure 7 compares the $N - \varepsilon$ curves of CFST without and with through-type cap gaps ($\chi = 2.1$, 4.2, and 6.3%).

As shown in Fig. 7, all CFSTs with or without cap gaps are presented typical strain-softening properties. The results complied with those of Refs. [14] and [15]. There were two yield points at $\chi = 6.3\%$ corresponding to $N - \varepsilon$ curves at peak

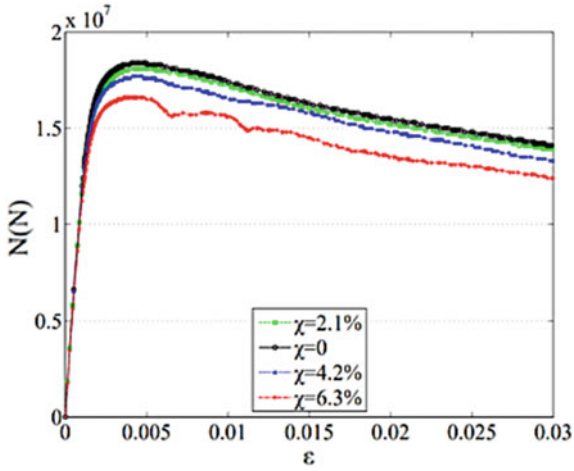


**Fig. 7** Comparison of $N$ versus $\varepsilon$ relations

load, where $\varepsilon$ yield stopped, and thereafter, two steps referred to strain-hardening again. The $N$ in CFST with cap gaps was suddenly reduced after peak load; However, when $\chi = 4.2\%$ and 2.1% or when there were no cap gap defects, CFST $N - \varepsilon$ curves presented a smooth shape. Thereafter, when CCC came into contact with external SWTs, $N$ was increased again. Figure 8 compares typical CFST failure modes. Elephant foot-shaped buckling deformation was magnified by 2 times to more clearly show deformed. This type of deformation was observed in CFST upper half. It is noteworthy that, in CFSTs with $\chi = 2.1\%$, a slight elephant foot-shaped buckling deformation was witnessed, while in those with $\chi = 4.2$ and 6.3%, many large deformations were observed. The results showed that large gaps resulted in greater spaces for local buckling deformations of CFST. CCC deformation shapes are presented in Fig. 9. It was observed that CCC had various bending deformation modes at various depths of cap gap.

With the increase of the depth of cap gap, stress and bending deformation were concentrated in compression zone and CFSTs presented local fractures and brittle failure stages.

It was noted that before the interaction of CCC and external SWTs, the greatest concrete cross-sectional deformation took place in the upper half. After that, when CCC came into contact with external SWTs, CCC cross-sectional deformation at compression region was confined by SWT. Therefore, CCC cracking position moved toward the mid-height of CFST. Concrete failure was witnessed at regions where local buckling of SWT occurred, as shown in Fig. 9.


**Fig. 8** Deformation modes of CFST. **a** $\chi = 2.1\%$, **b** $\chi = 4.2\%$, **c** $\chi = 6.3\%$

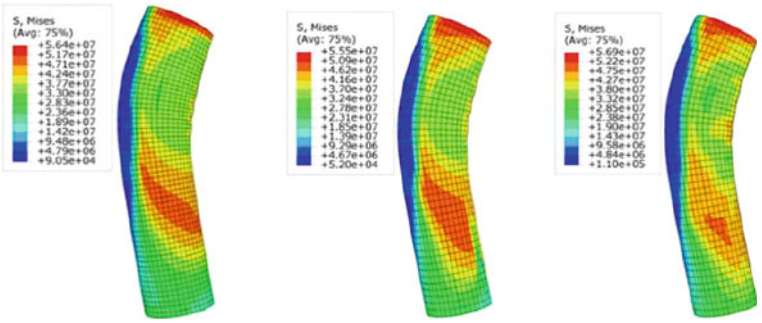


**Fig. 9** Concrete Mises stresses in CFSTs with various cap gap depths. **a** $\chi = 2.1\%$, **b** $\chi = 4.2\%$, **c** $\chi = 6.3\%$

## 4.3 FEA of CFSTs and Cap Gap with SWS Composite Defects

Figure 10 presents the comparison of $\chi - N - \varepsilon$ curves of CFSTs with through-type cap gaps ($\chi = 2.1$, 4.2, and 6.3%) in three dimensions.

It was observed that all CFSTs revealed typical smooth strain-softening properties in the absence of cap gap and SWS strength defects, which complied with the findings of [14] and [15]. Stress yield steps took place in the presence of cap gaps in CFST, as reported in [10] and [11]. This was the same as the results shown in Fig. 7. However, in the presence of composite defects effects at different levels of SWS strength, $N - \varepsilon$ curves of each of the components presented various rule of variation. By the decrease of the strength of SWS, yield step length and number on the $N - \varepsilon$ loss curves were increased. The results showed that $N - \varepsilon$ loss curves of CFST weld seam strength was gradually increased after peak strength. To the main reason for

**Fig. 10** $\chi - N - \varepsilon$-curves

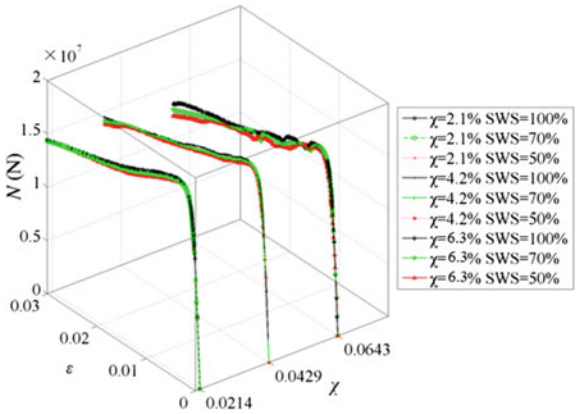

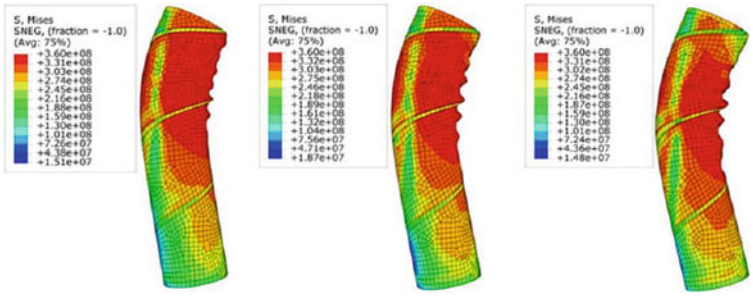


**Fig. 11** Tube Mises stresses (Pa) in CFSTs with 70% SWS strength. **a** $\chi = 2.1\%$, **b** $\chi = 4.2\%$, **c** $\chi = 6.3\%$

this was the weakening of local steel tube restraint ability on concrete by SWS, which decreased CFST composite bearing capacity.

Figure 11 compares typical failure modes of CFST with 70% SWS intensity under different cap gap defects. To obtain a clearer deformed image, elephant foot-shaped buckling deformations, which were found near the upper part of CFST, were multiplied by 2.

It should be noted that, for CFSTs with $\chi = 2.1\%$, slight elephant foot-shaped buckling deformations were only observed, while for those with $\chi = 4.2\%$ and 6.3%, such deformations were more intense, as shown in Fig. 8. Unlike intact SWS, however, the shape and location of local buckling in such steel tubes were different.

In defected SWS, steel tube tensile yielding position was observed at the first welding seam, regardless of the value of $\chi$. Along with first weld line, by increasing $\chi$ value, compressive yield also occurred on the steel tube of compressive side. As shown in Fig. 11, in case the strength of SWS was equal to 70% of the ideal value and $\chi$ was tripled from 2.1 to 6.3%, first SWS tensile yield on the upper part of CFST on tensile side was transferred to folding failure on compression side along SWS rotation direction. This showed that SWS defects were the main reason for the bending failure of CFST.

## 5 Conclusions

(1) Based on the ultrasonic scanning experimental measurements of Chang-Qing Hun River Bridge, a composite FEA was developed for CFST exposed to eccentric axial compressions. In comparison with the existing FEA methods, it was shown that this FEA is perfect in prediction accuracy.

(2) Through the comparison of test results, it was found that SWS defects had weaker influence on the bearing capacity of CFST than on that of EST, especially in the absence of defect in internal concrete. However, SWS defect had a

significant influence on CFST local yield failure mode and outer SWT strength was decreased at weld seam.

(3) Considering single defect of cap gap, comparison of $N - \varepsilon$ curves showed that CFSTs with and without cap gaps had typical strain-softening characteristics. However, for CFSTs with high $\chi$ values, several yield points appeared on $N - \varepsilon$ curves due to multiple contacts between core concrete and outer SWTs.

(4) Comparing typical failure modes of CFSTs with single cap gap defect showed that cap gaps changed the pattern of CFST buckling deformation and larger gaps expanded local buckling deformation space of CFST.

(5) For CFSTs with cap gap and SWS composite defects, SWS defects weakened local steel tube restrain capacity to concrete, resulting in CFST bending failure. However, for CFSTs with the same level of SWS defects, tensile yield on the tensile side was transferred to compression side followed the rotation direction of the SWS, which indicated that welding defect degree significantly affected local failure mode.

**Acknowledgements** This research was supported by Liaoning Revitalization Talents Program (No. XLYC1907121), Province Natural Science Foundation of Liaoning, China (No. 20180550442), and Scientific Research Project of Liaoning Provincial Department of Education, China (No. lnjc202019, No. lnjc201904).

## References

1. Zheng, J.L., Wang, J.J.: Concrete-filled steel tube arch bridges in China. Engineering **4**, 143–155 (2018)
2. Han, L.H., Yao, G.H., Tao, Z.: Performance of concrete-filled thin-walled steel tubes under pure torsion. Thin-Walled Struct. **45**(1), 24–36 (2007)
3. Ellobody, E., Young, B.: Nonlinear analysis of concrete-filled steel SHS and RHS columns. Thin-Walled Struct. **44**(8), 919–930 (2006)
4. Hassanein, M.F.: Numerical modeling of concrete-filled lean duplex slender stainless steel tubular stub columns. J. Constr. Steel Res. **66**(8), 1057–1068 (2010)
5. Tao, Z., Uy, B., Liao, F.Y.: Nonlinear analysis of concrete-filled square stainless steel stub columns under axial compression. J. Constr. Steel Res. **67**, 1719–1732 (2011)
6. Tao, Z., Uy, B., Han, L.H., Wang, Z.B.: Analysis and design of concrete-filled stiffened thin-walled steel tubular columns under axial compression. Thin-Walled Struct. **47**(12), 1544–1556 (2009)
7. Ellobody, E., Young, B.: Design and behaviour of concrete-filled cold-formed stainless steel tube columns. Eng. Struct. **28**, 716–728 (2006)
8. Hu, H.T., Su, F.C.: Nonlinear analysis of short concrete-filled double skin tube columns subjected to axial compressive forces. Marine Struct. **24**, 319–337 (2011)
9. Huang, H., Han, L.H., Tao, Z., Zhao, X.: L: Analytical behaviour of concrete-filled double skin steel tubular (CFDST) stub columns. J. Constr. Steel Res. **66**(4), 542–555 (2010)
10. Liao, F.Y., Han, L.H., He, S.H.: Behavior of CFST short column and beam with initial concrete imperfection. Experiments. J. Constr. Steel Res. **67**(12), 1922–1935 (2011)
11. Liao, F.Y., Han, L.H., Tao, Z.: Behavior of CFST stub columns with initial concrete imperfection: Analysis and calculations. Thin-Walled Struct. **70**, 57–69 (2013)

12. Han, L.H., Hou, C.C., Wang, Q.L.: Behavior of circular CFST stub columns under sustained load and chloride corrosion. J. Constr. Steel Res. **103**, 23–26 (2014)
13. Huang, Y.H., Liu, A.R., Fu, J.Y., Pi, Y.L.: Experimental investigation of the flexural behavior of CFST trusses with interfacial imperfection. J. Constr. Steel Res. **137**, 52–65 (2017)
14. Gunawardena, Y., Aslani, F.: Behaviour and design of concrete-filled mild-steel spiral welded tube short columns under eccentric axial compression loading. J. Constr. Steel Res. **151**, 146–173 (2018)
15. Gunawardena, Y., Aslani, F.: Finite element modelling of axial loaded mild-steel hollow spiral-welded steel tube short columns. In: Proceedings of 9th International Conference on Advances in Steel Structures, vol. 1, pp. 1559–1570, Hong Kong (2018)
16. Ding, Q.J.: Application of large-diameter and long-span micro-expansive pumping concrete filled steel tube arch bridge. J. Wuhan Univ. Technol.-Mater. Sci. **4**, 11–15 (2001)
17. Ramos, A.G., Jacob, J., Justo, J.F., Oliveira, J.F., Rodrigues, R., Gomes, A.M.: Cargo dynamic stability in the container loading problem -a physics simulation tool approach. Int. J. Simul. Process Model. **12**(1), 29–41 (2017)
18. Wang, H.X., Chen, S.S., Liu, Y.X., Zhang, L.J., Zhang, Z.N.: Numerical simulation and experimental validation for design improvement of packer rubber. Int. J. Simul. Process Model. **12**(5), 419–428 (2017)
19. Tao, Z., Wang, X.Q., Uy, B.: Stress-strain curves of structural and reinforcing steels after exposure to elevated temperatures. J. Mater. Civ. Eng. **25**, 1306–1315 (2013)
20. American Concrete Institute: Building Code Requirements for Structural Concrete (ACI 318-11) and Commentary. Farmington Hills, MI, USA (2011)
21. Papanikolaou, V.K., Kappos, J.: Confinement-sensitive plasticity constitutive model for concrete in triaxial compression. Int. J. Solids & Struct. **44**(21), 7021–7048 (2007)
22. Mander, J.B., Priestley, M.J.N., Park, R.: Theoretical stress-strain model for confined concrete. J. Struct. Eng. **114**, 1804–1826 (1988)
23. Mander, J.B., Priestley, M.J.N., Park, R.: Observed stress-strain behavior of confined concrete. J. Struct. Eng. **114**, 1827–1849 (1988)
24. Han, L.H., An, Y.F.: Performance of concrete-encased CFST stub columns under axial compression. J. Constr. Steel Res. **93**, 62–76 (2014)